JMEPEG (2015) 24:1669–1678
DOI: 10.1007/s11665-015-1441-1

1059-9495/$19.00

Corrosion and Tribocorrosion Performance of Thermally Oxidized Commercially Pure Titanium in a 0.9% NaCl Solution

R. Bailey and Y. Sun

(Submitted September 23, 2014; in revised form December 18, 2014; published online February 21, 2015)

In the present work, the corrosion and tribocorrosion characteristics of thermally oxidized commercially pure titanium in a 0.9% NaCl solution have been investigated. Thermal oxidation (TO) of CP-Ti was carried out at a temperature of 625 °C for 20 h. This treatment results in a multi-layered structure consisting of a 1 µm rutile (TiO_2) film and a 9 µm α-titanium oxygen diffusion zone (ODZ) (α-Ti(O)). Electrochemical tests were carried out on surfaces created at various depths from the TO-Ti original surface. It was found that the rutile film generated through TO offers excellent corrosion resistance over that of untreated Ti. Testing also provided evidence that oxygen content in the upper part of the ODZ (depths <5 µm from the surface) helps accelerate passive film formation and thus reduce the corrosion of CP-Ti. Tribo-electrochemical testing of TO-Ti was carried out against an alumina counter face under a load of 2 N and various anodic and cathodic potentials. It is initially shown that the rutile oxide layer offers both low friction and much better resistance to material removal during tribocorrosion than untreated CP-Ti. During sliding wear at open circuit potential, four frictional zones can be identified in a typical friction curve, each having its own characteristics corresponding to the oxide layer, the gradual or partial removal of the oxide layer, the diffusion zone, and the substrate. An unusual anodic protection behavior of the oxide film has also been observed. When the TO-Ti is polarized anodically during sliding, the durability of the oxide layer is prolonged, resulting in low friction and much reduced material loss. When cathodically charged to -1500 mV_{SCE} during sliding, both the TO-Ti and untreated CP-Ti experience a reduction in material loss. This is believed to be related to hydrogen evolution and titanium hydride formation.

Keywords corrosion, thermal oxidation, titanium, tribocorrosion, wear

1. Introduction

Titanium is a desirable engineering material due to its combination of lightweight, high strength, and excellent corrosion resistance. However, titanium is notorious for its poor tribological properties, which have restricted its uses to mostly non-tribological applications, due to the severe galling problem encountered in sliding contacts, producing large wear rates and the possibility of seizure (Ref 1, 2). Thermal oxidation is an effective method to overcome such issues.

Titanium owes its excellent corrosion resistance to a naturally occurring titanium dioxide film (1.5-10 nm thick) that instantaneously forms at the surface (Ref 3). Thermal oxidation allows for the expansion of this film. It has been shown that the rutile layer generated by thermal oxidation offers enhanced tribological and anti-corrosion properties over untreated titanium (Ref 1, 2, 4-6). Previous studies have shown that thermal oxidation produces a multi-layered structure atop of the bulk titanium, comprising a hardened oxygen diffusion zone (ODZ) and a rutile oxide layer (TiO_2) at the surface (Ref 7-9). The oxide layer has a tendency to delaminate from the substrate due to the high internal stresses built up in the layer during thermal oxidation. This is especially true when thicker layers are generated by oxidation at high temperatures or for prolonged times (Ref 5, 10, 11). It has been observed that an oxidation temperature between 600 and 650 °C offers the best combination between oxide layer thickness and adhesion (Ref 2, 10, 12).

The tribological characterization of thermally oxidized titanium has previously been investigated under dry (Ref 7) and lubricated conditions (Ref 1, 10, 13-16). These studies identified the effect of structural composition on the friction and wear response of thermally oxidized titanium. Several studies have also been conducted on the corrosion behavior of thermally oxidized titanium (Ref 8, 9, 13). It has been confirmed that the oxide layer provides additional protection against corrosion by serving as a barrier layer (Ref 17). However, all the reported corrosion tests were conducted on the as-oxidized surface. Since the oxide layer is prone to de-lamination from the surface during service, it is important to understand the corrosion characteristics of the ODZ as a function of depth from the surface after the oxide layer is removed. This forms one of the objectives of the present investigation.

Another major consideration in the use of titanium is the interaction between wear and corrosion, i.e., tribocorrosion, such as in medical implants, valves, and marine applications, where wear can cause the damage of the passive film on the contact surface, leading to accelerated corrosion, which in turn can cause accelerated wear (Ref 18-23). Although the

R. Bailey and **Y. Sun,** School of Engineering and Sustainable Development, Faculty of Technology, De Montfort University, Leicester, UK. Contact e-mail: p08293800@myemail.dmu.ac.uk.

tribocorrosion behavior of thermally oxidized titanium has been investigated by several investigators (Ref 14, 21, 24), none of these studies have identified the relative contribution of the oxide layer and the ODZ. Thus, another objective of the present investigation is to clarify the effect of each substructure of the oxidized layer on tribocorrosion.

Therefore, in the present work, experiments were conducted to investigate the corrosion behavior of thermally oxidized titanium in 0.9% NaCl solution as a function of depth from the surface by mechanically removing successive layers across the oxidized layer. Tribocorrosion tests were also conducted under combined sliding wear and electrochemical conditions at various applied potentials. The results obtained from the experiments are reported and discussed in this paper.

2. Experimental

2.1 Material and Sample Preparation

Commercially pure titanium (CP-Ti) grade 2 (Ti/<0.1C/<0.3Fe/<0.015H/<0.03N/<0.25O) was used as the substrate material. Samples of 20 mm × 20 mm × 2 mm were prepared by cutting an as-received CP-Ti plate. The samples were then manually ground using progressively finer SiC grinding papers down to the P1200 grade. The resulting surface finish was investigated using a stylus profilometer and showed an average roughness of 0.203 μm (R_a). The samples were then ultrasonically cleaned in methanol for 15 min.

Thermal oxidation was then carried out using a muffle air furnace at a temperature of 625 °C and for 20 h. The samples were then allowed to furnace cool to room temperature. These parameters have been proven to create an adherent rutile oxide layer and an ODZ beneath (Ref 7). Figure 1 shows the cross-sectional morphology of the oxidized sample, together with the oxygen concentration profile measured across the oxidized layer by glow discharge spectrometry. Table 1 lists the measured layer thickness, surface hardness, and roughness values for the oxidized and untreated titanium. These data were compiled from a previous study using the same conditions (Ref 7). The oxide layer is about 1-μm thick with a high oxygen concentration close to TiO_2 stoichiometry. Below this oxide layer is the ODZ of about 9-μm thickness with a gradually decreasing oxygen concentration. Thermal oxidation effectively hardens the surface of CP-Ti and leads to a marginal increase in surface roughness. Full microstructural characterization has been carried out in a previous work (Ref 7).

2.2 Electrochemical Corrosion Tests

Electrochemical corrosion tests were performed using a Princeton applied research model K0235 three-electrode electrochemical flat cell connected to an ACM Gill AC potentiostat equipped with a data logger. The specimen was clamped to the cell, sealing against a PTFE (Polytetrafluoroethylene) knife-edged gasket, which exposes 1.0 cm^2 of the specimen surface to the electrolyte. A schematic of this setup is shown in Fig. 2(a). The reference electrode was a saturated calomel electrode (SCE), with all potentials referring to the SCE scale. The electrolyte used for all tests was 0.9% NaCl solution (pH ≈ 7), which was prepared from analytical grade chemicals and distilled water. All tests performed were conducted three times at standard room temperature (20 °C) open to the air. The

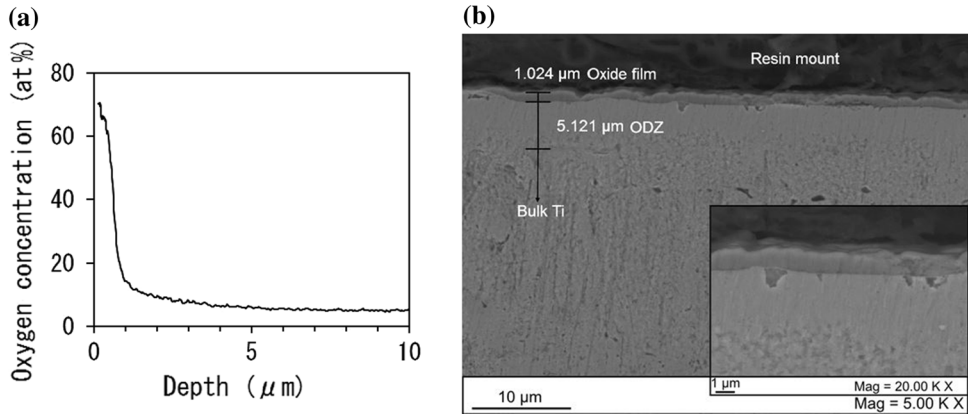

Fig. 1 (a) Oxygen concentration profile measured by Glow discharge spectroscopy (GDS) across oxide layer produced at 625 °C for 20 h on commercially pure titanium (CP-Ti) and (b) SEM image showing the cross-sectional structure of thermally oxidized CP-Ti

Table 1 Summary of layer thickness and hardness results for thermally oxidized and untreated CP-Ti [7]

Sample	Oxide layer thickness (μm)	ODZ thickness (μm)	Surface hardness(a)			Surface roughness R_a (μm)
			$HV_{0.05}$	$HV_{0.1}$	$HV_{0.2}$	
Untreated	<0.01(b)	0	298	298	282	0.203
Oxidized	0.98	4.95	766	563	431	0.211

(a)Measured using an Indentec ZHV microhardness tester on the as-oxidized surface (b)Estimated native oxide film

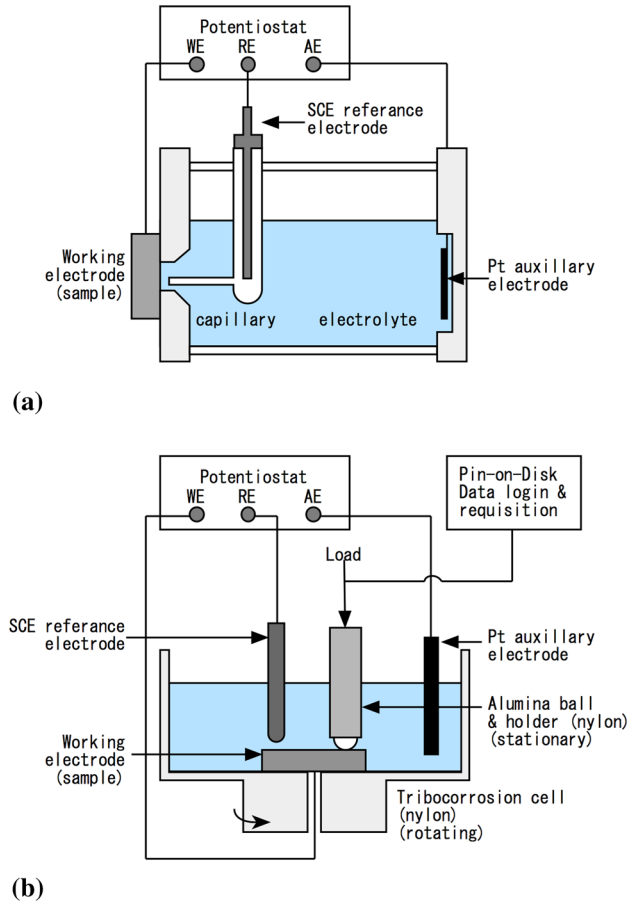

Fig. 2 Schematic diagrams showing (a) the arrangement of the electrochemical cell used during electrochemical depth profiling and (b) the tribo-electrochemical cell used during tribocorrosion testing

results are reproducible, and average values or the most representative data are presented in this paper.

Before electrochemical testing, progressive grinding of the thermally oxidized titanium was carried out using 1200P SiC Paper. This was to expose the underlying layers at various depths from the surface. 2-3 μm of material was removed with each stage of grinding.

In order to accurately measure the thickness of the removed material, the following measurements before and after surface grinding were used: Weighing the specimen using a balance accurate to 0.1 mg, measuring the size of the diagonals of a Vickers hardness indent made on the surface just outside the corrosion test area, and measuring the thickness of the specimen using a digital micrometer accurate to 1 μm. After cleaning ultrasonically in methanol for 5 min, each ground sample was then loaded into the electrochemical test cell and then cathodically charged at −500 mV for 3 min to create a uniform starting point for all samples. Each exposed layer was then tested using the following electrochemical techniques.

Potentiodynamic polarization measurement was performed using a sweep rate of 1 mV/s, starting from a cathodic potential of −400 mV (versus open circuit potential (OCP)), then to an anodic potential of 1500 mV (versus OCP). The corrosion current densities were determined by the Tafel extrapolation method. The OCP was determined during 30 min of stabilization prior to the potential sweep.

Current transient measurements were performed by potentiostatically polarizing the specimens at a constant potential of 500 mV_{SCE} for 3600 s. The variation in current density with time was recorded continuously throughout the test.

2.3 Tribocorrosion Tests

Tribocorrosion tests were carried out using a pin-on-disk tribometer modified to incorporate electrochemical testing, as shown in Fig. 2(b). Before the test, a test area of 1.23 mm^2 was isolated using insulating lacquer. During the test, the sample rotated against a stationary alumina (Al_2O_3 Grade 25) ball with a diameter of 8 mm manufactured by Trafalgar bearings. Alumina was chosen due to its hardness and inertness. The rotation speed of the sample was set to 60 rpm with a wear track diameter of 9 mm. A load of 2 N was applied for duration of 4 h with 30-min stabilization (cell rotation but no contact) time before and after sliding. This was to create a stable starting point for the samples and then to see the repassivation response once sliding had commenced. The tests were performed with a sliding speed of 2.8 cm/s and a total sliding distance of 408 m. All tests were carried out in a 0.9% NaCl solution at room temperature (20 °C), with samples potentiostatically polarized at potentials of +1000, +500, −900, and −1500 mV_{SCE}. OCP measurements were also taken. Wear depth and total material loss (TML) in volume from each sample were then analyzed using a stylus profilometer to measure the surface profiles across the wear track at 4 different locations. Wear track morphology was investigated using two different models of SEM (Carl Zeiss EvoHD 15 SEM and a Leica S430 SEM), and the specimens were investigated in secondary and back-scattered electron modes with an accelerating voltage of 12 kV.

All tests were carried out three times and were found to be reproducible. The mean results are presented in this paper.

3. Results and Discussion

3.1 Electrochemical Behavior as a Function of Depth from Surface

3.1.1 Potentiodynamic Behavior. Figure 3 shows anodic polarization curves for the thermally oxidized titanium at various depths from the as-oxidized surface, correlating to different amounts of oxygen within the substructure. The polarization curves show that the thermally formed oxide layer offer much enhanced corrosion resistance over untreated CP-Ti. The oxide layer offers an anodic shift in the free corrosion potential to −200 mV_{SCE} from approximately −450 mV_{SCE} for untreated CP-Ti. Along with the shift in corrosion potential, the oxide layer also shows very low current densities throughout the potential sweep. Both the anodic shift and low current densities have been reported previously (Ref 9, 13, 25). At 2 μm below the surface, the 1-μm-thick oxide layer has been fully removed and the ODZ is then exposed. The free corrosion potential and the corrosion current density of the ODZ are slightly shifted from that of the bulk material. Oxygen in the diffusion zone seems to have a slight positive effect on the corrosion properties of titanium through reduced current densities and higher corrosion potential (−350 mV_{SCE}). At further depths (5 μm and deeper) from the surface, the oxygen content is much reduced (Fig. 1a) and the material's electrochemical response shows a very reproducible and consistent polarization curve with a stable passive region between 200 and 1000 mV_{SCE}, where current density is stable at around

0.005 mA/cm^2, which is similar to that of untreated CP-Ti. The main benefit of thermal oxidation comes from the oxide layer and to a lesser extent from the upper part of the ODZ, with the bulk titanium retaining its corrosion properties.

3.1.2 Current Transient Behavior. Potentiostatic testing was carried out at various sample depths by applying a potential of 500 mV_{SCE} for 3600 s. According to Fig. 3, at this potential all samples are within the passive region. Figure 4 shows the current transient response for the samples in the Log (I) versus Log (t) scale. The point defect model (PDM) and the high field theory (HFT) are well-used models to describe the change in ion flux at the sample surface (Ref 26-28). As the surface passive film thickens, the ion flux is reduced, leading to lower conduction and therefore lower current densities. This current response over time is described by Eq 1 (Ref 27, 29, 30):

$$I = 10^{-[A+k\log(t)]}. \quad \text{(Eq 1)}$$

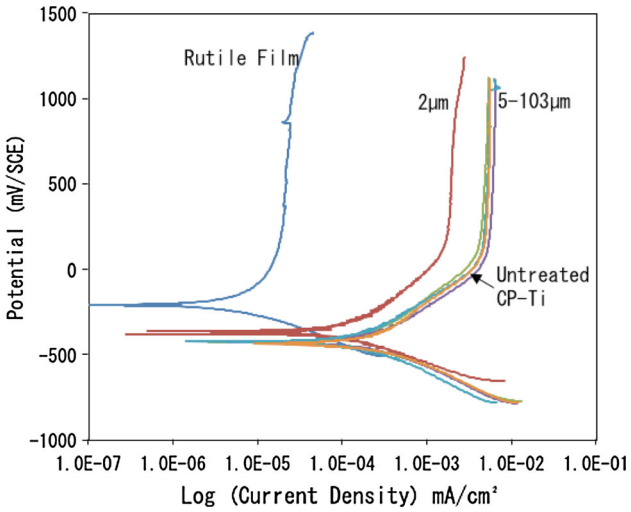

Fig. 3 Anodic polarization curves measured for thermally oxidized titanium at various depths from the treated surface, using a sweep rate of 1 mV/s in a 0.9% NaCl solution

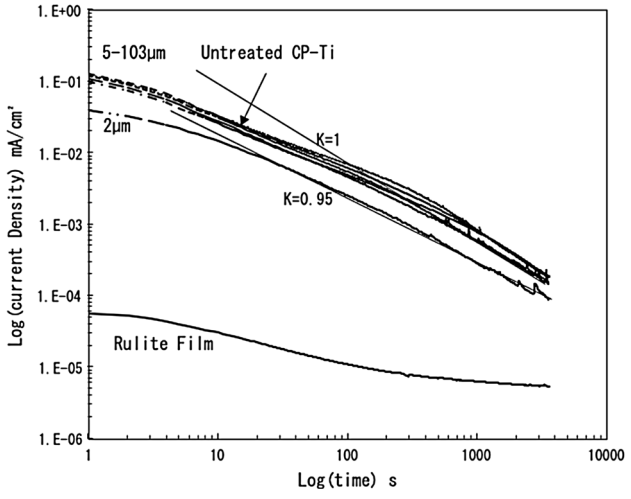

Fig. 4 Current transient curves in the log (I) vs. log (t) scale measured during film formation at various depths from the surface of thermally oxidized titanium. All tests were conducted at a potential of 500 mV for duration of 3600 s in a 0.9% NaCl solution

Using Eq 1, a plot of Log (I) against Log (t) should produce a straight line where the gradient = $-k$ and intercept at A when $t = 1$. If $k = 1$, this would be characteristic of a thick (greater than 0.5 nm) dense film; thinner, more porous films would have a $k < 1$ (Ref 27, 30).

In Fig. 4, the curves generated for the ground samples clearly conform to Eq 1. There exists an initial stage in all the tested samples where there are lower curve gradients ($k \approx 0.5$). This low value of k is attributed to small film thickness in the initial stage of polarization, a phenomenon that has been reported in previous studies (Ref 27, 30). As polarization time increases, the passive film thickens and the k value approaches 1. Once again, it can be observed that there is a variation between the current densities just below the thermally formed oxide layer (2 μm) and then deeper (5 μm-in words). At a depth of 2 μm, the curve reaches linearity sooner (after 50 s) than at deeper depths (approx. 200 s). There is also a difference in the linear slope gradients. The 2-μm-depth sample never reaches $k = 1$, whereas the further ground samples all achieve this ideal value. This variation in the time to reach the linear stage and final slope value shows that when there is high oxygen content within the titanium lattice, a stable passive film can be built up more quickly to result in the lower passivity current density (Fig. 4). This faster response at 2-μm depth could be attributed to the higher free corrosion potential and lower current densities as observed in Fig. 3. However, the data in Fig. 4 suggest that the film generated is less dense and slightly more porous than that produced when lower oxygen concentrations are present within the titanium substructure.

As can be clearly seen from Fig. 4, the oxide layer on the as-oxidized surface is a barrier layer which results in very low current densities. The current transient behavior of the as-oxidized surface does not comply with Eq 1 because a thick (1 μm) oxide layer already exists before the polarization test.

3.2 Tribocorrosion Behavior

3.2.1 Open Circuit Tribocorrosion Behavior. Initial tribocorrosion tests were carried out in an open circuit without externally applied potentials. The samples were tested for duration of 5 h, with 4-h sliding and 30-min stabilization before and after sliding. Figure 5 shows the evolution of potential and friction coefficient over time for the thermally oxidized sample. During tribocorrosion testing, four distinct frictional zones are observed. These friction zones have been observed during dry sliding of thermally oxidized CP-Ti in a previous study (Ref 7). It is proposed that each zone observed is related to the material composition and substructure. Thermal oxidation generates a layered structure, and the friction behavior is a response to each structure and the transition between these layers as wear progresses. The frictional zones relate to the following structural transitions: (I) oxide layer, (II) removal of the oxide layer, (III) ODZ, and (IV) bulk titanium. With the identification of these four frictional zones from the friction curves, it can be clearly seen that the OCP data show these corresponding zones.

OCP gives insight into the surface condition of the sample in real time during the sliding wear process. Each zone exhibits a unique friction and OCP response with differing levels of material activity, friction, and wear, as described below with reference to Fig. 5.

Zone I Sliding contact between the Al_2O_3 ball and the oxide layer results in low friction. Upon sliding, the OCP experiences a catholic shift from −200 to −500 mV_{SCE} and remains at

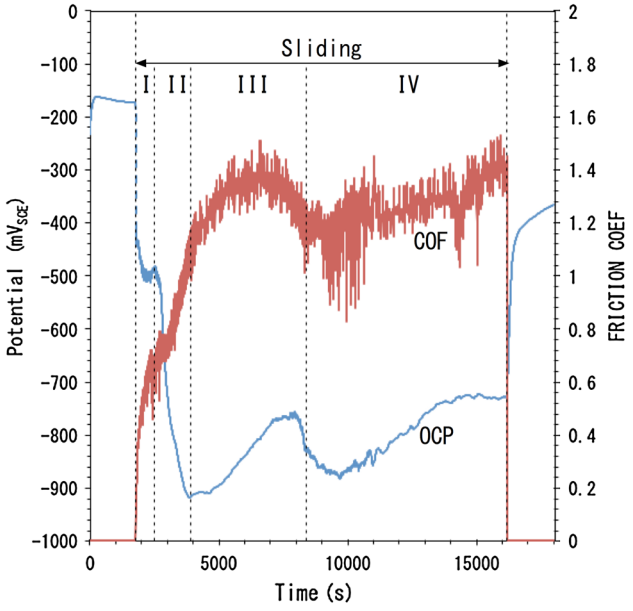

Fig. 5 Open circuit potential and coefficient of friction curves recorded for a contact load of 2 N in a 0.9% NaCl solution for thermally oxidized CP-Ti. The onset of sliding is indicated after 30-min stabilization. Four distinct frictional zones can be observed: (I) Oxide layer, (II) Partial removal of the oxide layer, (III) Oxygen diffusion zone, and (IV) Substrate

−500 mV_{SCE} for around 700 s. During this phase, wear occurs within the oxide layer, resulting in the observed low friction coefficient (<0.6) (Ref 7, 10) and a relatively small drop in OCP. Figure 6(a) shows the wear track produced after sliding wear test at OCP for 500 s. It can be seen that the oxide layer is not worn through and maintains its integrity with the substructure, and the dominant wear mechanism is micro-polishing of the oxide layer.

Zone II As sliding wear continues, the oxide layer is gradually removed or damaged, exposing areas of the ODZ from below. During this transitional zone, the OCP is gradually dropped from −500 to −900 mV_{SCE}. Along with this cathodic shift of OCP, the friction coefficient is gradually increased from 0.6 to 1.2. The wear mechanism changes from micro-polishing of the oxide layer in Zone I to delamination of the oxide layer and abrasive wear of the exposed ODZ, as can be clearly seen in Fig. 6(b).

Zone III Full exposure of the ODZ to sliding contact results in a large cathodic shift of OCP. The exposure of the ODZ coincides with a period of increased friction (μ = 1.2). While sliding occurs in the ODZ, the OCP is gradually shifted from −920 to −750 mV over a time period of approximately 3000 s. This is due to passive film formation within the wear track. With each successive pass of the alumina ball, the passive film is only partially removed. There becomes a time when the oxide film generated within the wear track is removed at a rate equal to or slower than the rate of oxide film formation. This is

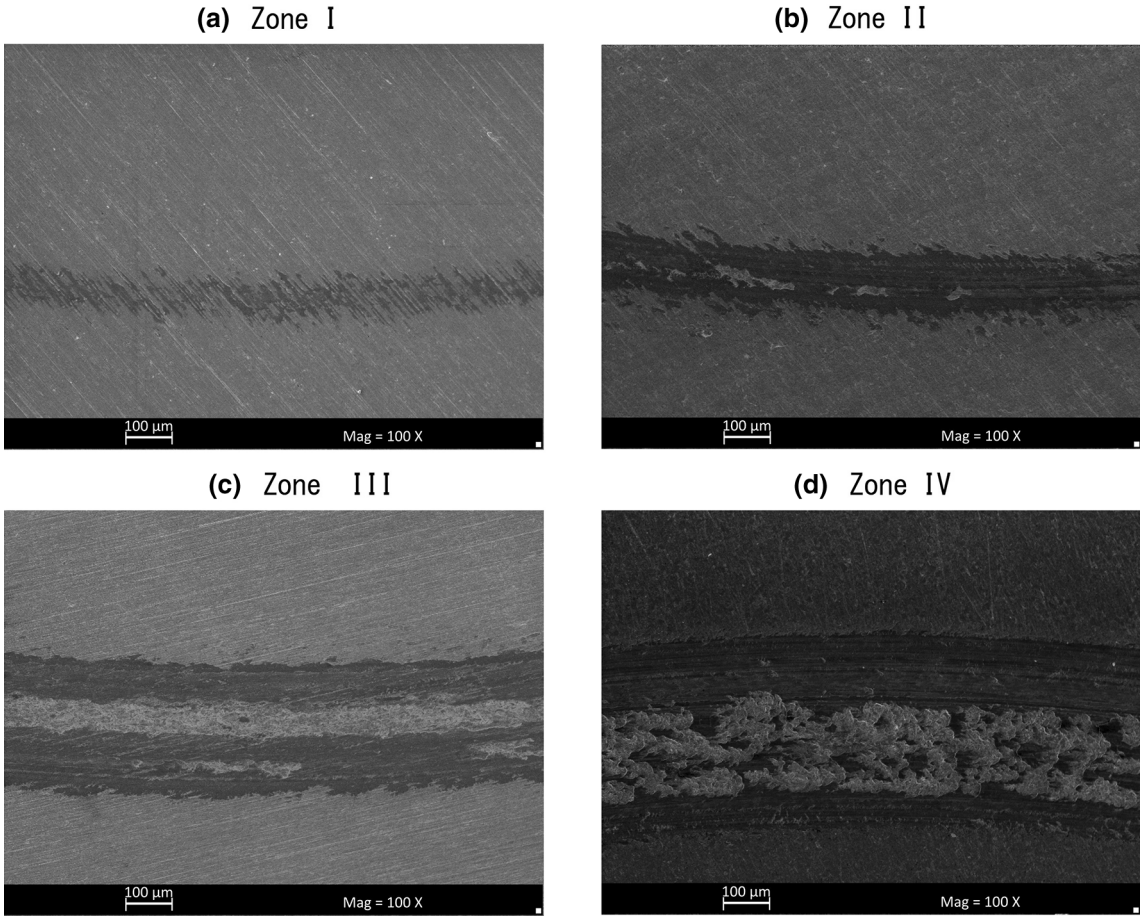

Fig. 6 SEM images showing wear track morphology of the OCP tribocorrosion tests after sliding durations of (a) 500 s, (b) 1700 s, (c) 4700 s, and (d) 14,400 s. The times selected represent the four frictional zones observed in this figure. All tests were subjected to a 2 N sliding load

shown by the stabilization of the OCP at the later stage of zone III. This removal and formation of the passive film can also explain the smooth nature of the wear track observed during this period of the test (Ref 7, 10, 24), shown in Fig. 6(c).

Zone IV Removal of the ODZ from the wear track allows for the exposure of the underlying bulk material. There is a reduction in friction coefficient as previously seen when in contact with untreated CP-Ti (Ref 5, 7). The OCP data show another cathodic shift as the ODZ is removed. But the OCP again shows a recovery over 4000 s. Microscopic examination of the wear track shown in Fig. 6(d) indicates a joint mechanical and chemical tribocorrosion response. At the outer edges, there is a smooth area in the wear track. This is associated with the fast passivation of the ODZ. This fast passivation results in a smooth polished surface. In the center of the wear track, typical wear morphology expected of titanium is observed with wear regimes dominated by severe adhesion and delamination (Ref 7, 10).

When considering the tribocorrosion response of thermally oxidized titanium at OCP, it is clear that the oxide layer offers the most effective protection against both corrosion and tribocorrosion, with the layer thickness being a restraining factor to the duration of protection. Once the oxide layer has been removed, the diffusion zone and bulk titanium have similar OCP response. However, the time taken for re-passivation is significantly less for the ODZ than for the bulk titanium. When relating this to the corrosion depth profiling analysis undertaken in section 3.1.2, it is clear that the passivation of the ODZ happens at a faster rate than that of bulk titanium. The ODZ offers improved passivation kinetics and reduced wear as compared to bulk titanium, with the drawback of having increased friction.

3.2.2 Effect of Applied Potential on Tribocorrosion Behavior. In order to understand the contributing factor of corrosion on the overall tribocorrosion behavior of thermally oxidized titanium, potentiostatic sliding wear tests were carried out at both anodic and cathodic potentials. Figure 7 shows the friction and current responses of the test sample at potentials of +1000, +500, −900, and −1500 mV_{SCE}. Clearly, applied potential has a large impact on the friction behavior of the thermally oxidized titanium.

Applying an anodic potential on a sample allows the anodic forward reactions to take place. For passive materials, this is normally associated with increased current at higher potentials. However, it can be seen in Fig. 7(a) (1000 mV_{SCE}) and (b) (500 mV_{SCE}) that sliding only leads to a small increase in current during the course of Zone I, and such an increase is even smaller at the higher potential. This lower current is in tandem with reduced friction coefficients observed throughout the test. As the reduced friction is associated with the thermally formed oxide layer (Zone I), it can be assumed that during these tests, this oxide layer stays in place longer and is removed at a more gradual rate than that observed under OCP conditions. As discussed earlier, Zone I (the oxide layer) lasts about 700 s at OCP (Fig. 5). At the anodic potential of 500 mV_{SCE}, Zone I lasts much longer, about 4000 s (Fig. 7b). When the anodic potential is increased to 1000 mV_{SCE}, Zone I is further extended to nearly 10,000 s. Clearly increasing anodic potential

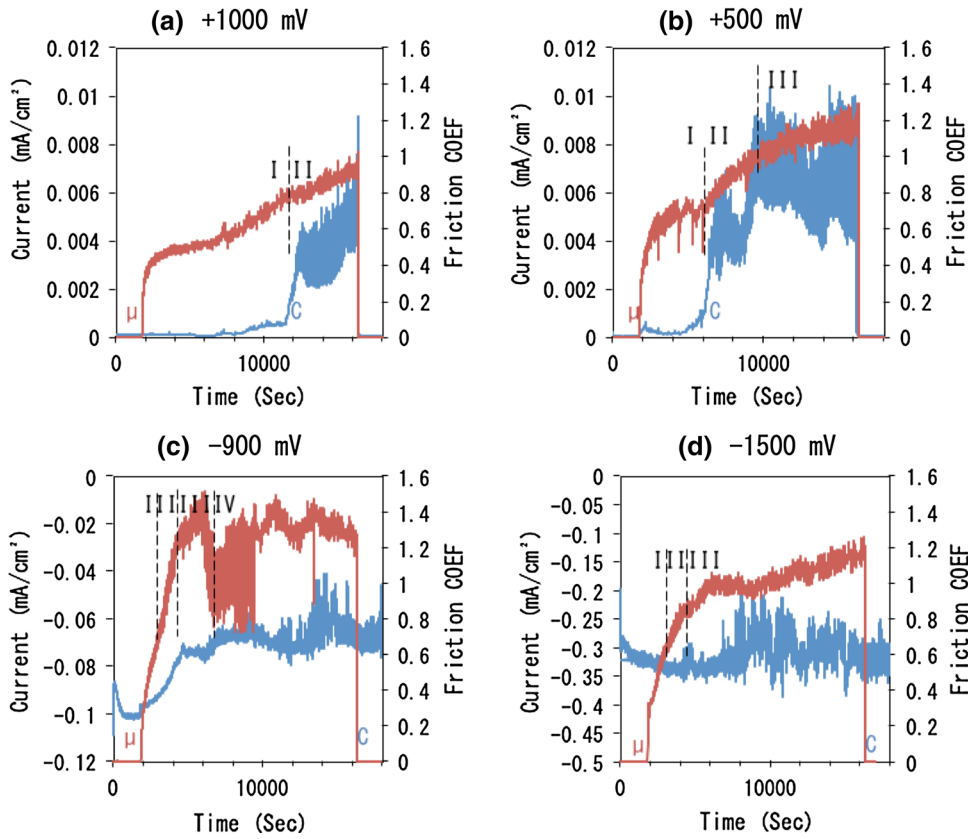

Fig. 7 Friction coefficient (μ) and current density (I) against time for tribocorrosion testing at potentials of (a) 1000 mV, (b) 500 mV, (c) −900 mV, and (d) −1500 mV. Frictional zones identified: (I) oxide layer, (II) partial removal of the oxide layer, (III) oxygen diffusion zone, and (IV) substrate. Sliding contact was initiated for 4 h, with a 30-min settling period before and after sliding

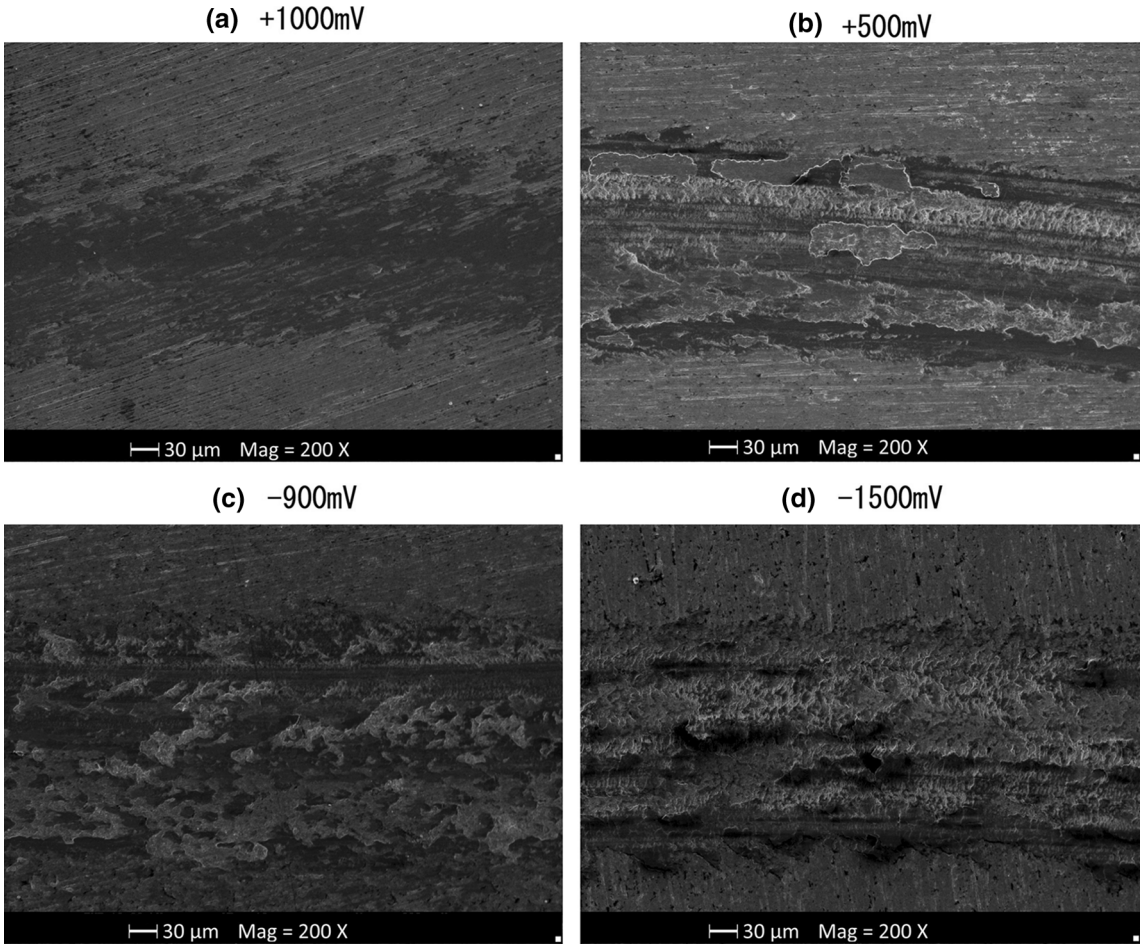

Fig. 8 SEM images showing the wear track morphology produced on the thermally oxidized titanium, after tribocorrosion testing at potentials of +1000 mV (a), +500 mV (b), −900 mV (c), and −1500 mV (d). All tests were conducted using a load of 2 N for 14,400 s

helps increase the durability of the thermally formed oxide layer on CP-Ti and thus to reduce friction and chemical wear. The wear track morphologies shown in Fig. 8(a) and (b) for the 1000 and 500 mV_{SCE} wear tracks are also substantially different from those observed after the OCP tests (Fig. 6d). At the potential of 1000 mV_{SCE} (Fig. 8a), the wear track exhibits wear mechanisms dominated by micro-polishing of the thermally formed oxide layer (Zone I) with some slight delamination of the layer and exposure of the underlying ODZ (Zone II), indicating that Zone I dominates the sliding wear process. At 500 mV_{SCE}, the wear track morphology shows large-scale delamination of the oxide layer and large exposure of the ODZ (Zone III) (Fig. 7b). No exposure of the bulk Ti (Zone IV) is observed at these two anodic potentials.

It is usually expected that when the potential of the system is moved to a value in a cathodic direction from OCP, material loss is solely due to the mechanical wear process, as the negative charge removes the ability for the formation of positive metal ions. This is shown through the flow of a negative current (Ref 31). Figure 7c shows the friction and current response when a cathodic potential of −900 mV_{SCE} is applied to the sample. The friction curve observed is very similar to that at OCP in Fig. 5, characterized by the four-zone mechanism described previously. The thermally formed oxide layer, which lasts for only 600 s (Zone I) is damaged quickly by the mechanical action. Wear track morphology, as shown in Fig. 8(c), is seen to be dominated by severe abrasion and adhesive wear. When looking at how this wear track differs from that at OCP shown in Fig. 6(d), there are no longer the smooth sides associated with passivation of the ODZ. This is as expected due to lack of anodic oxidation at cathodic potentials.

Tribocorrosion tests were conducted at a further cathodic potential of −1500 mV_{SCE}. At such a potential, the evolution of hydrogen is predicted (Ref 32-36). Hydrogen is able to penetrate into titanium, causing the formation of titanium hydride (TiH_2). The friction and current responses shown in Fig. 7(d) indicate that initial removal of the thermally formed oxide layer occurs at the same rate as at −900 mV_{SCE} (Fig. 7c), but once the oxide layer has been removed, there is a stabilization of the frictional response, rather than the peak and drop associated with the wear of the ODZ (zone III to zone IV in Fig. 5), indicating that the ODZ has not been worn through during the test (no zone IV). When looking at the wear track morphology shown in Fig. 8(d), there is a substantial difference in wear mechanisms involved. The wear track is now littered with cracks and dominated by abrasive wear with the polishing of the peaks, as observed in a previous tribocorrosion study of a titanium alloy when hydride was formed under cathodic conditions (Ref 37). It is interesting to note that once the load has been removed, there is no reduction in cathodic current flowing in the sample, indicating that the evolution of hydrogen continues after sliding.

3.2.3 Total Material Loss Rate. TML from the wear track was measured using a profilometer, which was then normalized with total sliding distance and applied load to obtain specific total material loss rate (TMLR). The results are shown in Fig. 9 as a function of applied potential for the thermally oxidized and untreated CP-Ti samples. TML in volume (V_{total}) is a sum of both mechanical (V_{mech}) and chemical (V_{chem}) volume losses, i.e.,

$$V_{total} = V_{mech} + V_{chem}. \quad \text{(Eq 2)}$$

Faraday's law can be used to determine the contribution of chemical wear in the tribocorrosion process. The anodic current detected during tribocorrosion testing is related to the amount of material lost due to anodic oxidation and/or dissolution through the Faraday's law (Ref 28, 31, 38, 39):

$$V_{chem} = ItM/nF\rho, \quad \text{(Eq 3)}$$

where I is the average current (A) developed during sliding contact, t is the time (s) of sliding contact, F is Faraday's constant (964858.34 As/mol), M is the atomic mass of the metal (47.767 g/mol for Ti), n is the charge number for the oxidation reaction (valance = + 4 for Ti (Ref 40)), and ρ is the density of the metal (4.11 g/cm^3).

From Fig. 9, several observations can be made regarding the effects of thermal oxidation on the tribocorrosion response of titanium and the effect of potential on TMLR. First, thermal oxidation reduces the TMLR across the spectrum as compared to untreated CP-Ti by an order of magnitude at OCP and cathodic potentials when mechanical wear is predominant. Such a beneficial effect of thermal oxidation is more significant at the anodic potentials, where a reduction in TMLR by nearly two orders of magnitude is seen due to the reduction in both mechanical and chemical wear.

Second, the effect of potential on TMLR of the oxidized CP-Ti is different from that of the untreated CP-Ti and many other materials reported (Ref 38, 41). For the untreated CP-Ti, as expected the TMLR increases with the increasing potential due to increased chemical wear. But at the cathodic potential of −1500 mV_{SCE}, the TMLR is much reduced, presumably due to the formation of titanium hydride. On the other hand, for the thermally oxidized CP-Ti, as the potential is increased from OCP, the TMLR is reduced, by nearly an order of magnitude at 1000 mV_{SCE}, which is not usually expected. This is due to the prolonged durability of the thermally formed oxide layer (Fig. 7a and b) relative to the tests at OCP (Fig. 5) and at cathodic potentials (Fig. 7c and d). This prolonged oxide layer coverage offers beneficial protection from both mechanical and

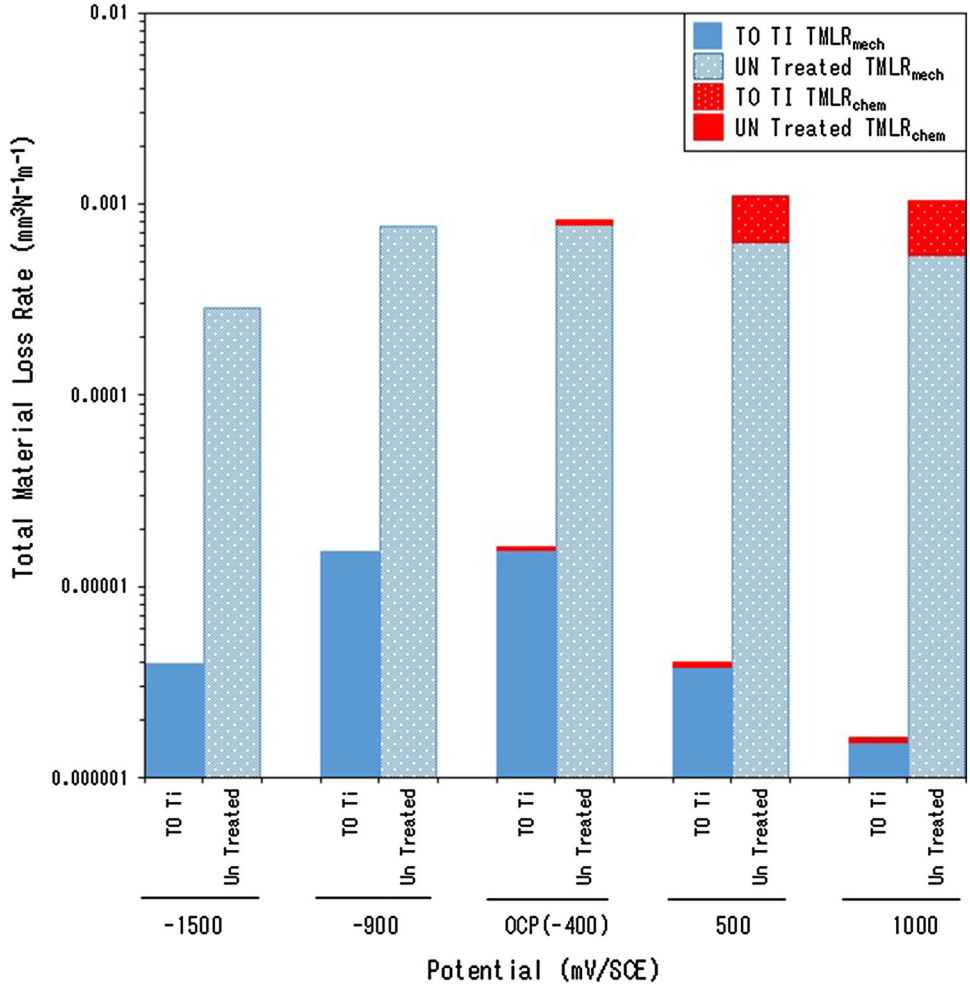

Fig. 9 Contribution of mechanical wear and corrosion to total material loss rate volume of thermally oxidized titanium and untreated titanium. All tests were conducted in a 0.9% NaCl solution

chemical wear. Such an anodic protection of the thermally formed oxide layer has not been reported previously. The reasons behind such an anodic protection are not clear at this stage. It is believed that applying an anodic potential to the samples increases the rate at which the exposed ODZ forms a passive film. When the thermally formed oxide layer begins to breakdown, rapid passivation of the exposed ODZ would reduce the internal stresses on any oxide layer remaining in place by filling cracks or gaps produced in the layer. This shows that if the adhesion between the thermally formed oxide layer and the underlying substructure can be addressed, thermal oxidation can offer a viable method to reduce wear and corrosion of CP-Ti.

Finally for the oxidized sample, when the potential is shifted cathodically from OCP to $-900\ mV_{SCE}$, the difference in TMLR is associated with the chemical wear induced at OCP. This is as expected due to the absence of chemical wear at the cathodic potential. A further higher cathodic potential of $-1500\ mV_{SCE}$ allows for the hydrolysis of water and the production of hydrogen. Absorption and diffusion of hydrogen into titanium at this potential is expected and the creation of a small hydrogen diffusion zone (HDZ) cannot be ruled out. However, the solubility limit of hydrogen in α-Ti is as low as 20-150 ppm (Ref 32, 42); excess hydrogen that is adsorbed above the solubility limit will form various hydride phase precipitates in the wear tracks. This formation of titanium hydride is known to induce hydrogen embrittlement and is usually associated with reduced mechanical properties of titanium (Ref 43, 44). However, the formation of hydride also induces real-time hardening within the wear track and could be accountable for the reduced TMLR measured for both the thermally oxidized and untreated CP-Ti under the relatively small contact load of 2 N employed in this work.

4. Conclusions

(1) The oxide layer produced by thermal oxidation serves as a barrier layer to improve the corrosion resistance of CP-Ti by reducing anodic currents and increasing corrosion potential.
(2) The high oxygen content in titanium lattice in the upper part of the ODZ helps accelerate passive film formation and thus to reduce corrosion of CP-Ti.
(3) During sliding wear at open circuit in 0.9% NaCl solution, four frictional zones can be identified in a typical friction curve, each having its own characteristics corresponding to the oxide layer, the gradual or partial removal of the oxide layer, the diffusion zone, and the substrate. Each zone has a characteristic response to OCP change during sliding.
(4) The thermally formed oxide layer offers both low friction and much better resistance to material removal during tribocorrosion than untreated CP-Ti.
(5) The thermally formed oxide layer exhibits unusual anodic protection behavior. When the thermally oxidized titanium is polarized anodically during sliding, the durability of the oxide layer is prolonged, resulting in low friction and much reduced TMLR. This is in contrast to the results obtained from the untreated CP-Ti and is believed to be due to the fast passivation of the exposed ODZ.
(6) Both the thermally oxidized and untreated CP-Ti experience a reduction in TMLR when cathodically charged to $-1500\ mV_{SCE}$ during sliding. This is believed to be related to hydrogen evolution and titanium hydride formation.

Acknowledgments

One of the authors (RB) would like to acknowledge the financial support of De Montfort University for providing a PhD scholarship. Special thanks are also due to The Alderman Newton's Educational Foundation, The Sidney Perry Foundation, and The Wyvernian Foundation for providing additional financial support during the course of this work.

References

1. A. Bloyce, P.Y. Qi, H. Dong, and T. Bell, Surface Modification of Titanium Alloys for Combined Improvements in Corrosion and Wear Resistance, *Surf. Coat. Technol.*, 1998, **107**(2–3), p 125–132
2. H. Dong and T. Bell, Enhanced Wear Resistance of Titanium Surfaces by a New Thermal Oxidation Treatment, *Wear*, 2000, **238**(2), p 131–137
3. Y. Sul, C.B. Johansson, Y. Jeong, and T. Albrektsson, The Electrochemical Oxide Growth Behaviour on Titanium in Acid and Alkaline Electrolytes, *Med. Eng. Phys.*, 2001, **23**(5), p 329–346
4. F. Borgioli, E. Galvanetto, F. Iozzelli, and G. Pradelli, Improvement of Wear Resistance of Ti-6Al-4V Alloy by Means of Thermal Oxidation, *Mater. Lett.*, 2005, **59**(17), p 2159–2162
5. D. Siva Rama Krishna, Y.L. Brama, and Y. Sun, Thick Rutile Layer on Titanium for Tribological Applications, *Tribol. Int.*, 2007, **40**(2), p 329–334
6. S. Banfield, J.C. Avelar-Batista Wilson, G. Cassar, A. Leyland, A. Matthews, and J. Housden, An Investigation into the Effect of Triode Plasma Oxidation (TPO) on the Tribological Properties of Ti6Al4V, *Surf. Coat. Technol.*, 2011, **206**(7), p 1955–1962
7. R. Bailey and Y. Sun, Unlubricated Sliding Friction and Wear Characteristics of Thermally Oxidized Commercially Pure Titanium, *Wear*, 2013, **308**(1–2), p 61–70
8. A.R. Shankar, N.S. Karthiselva, and U.K. Mudali, Thermal Oxidation of Titanium to Improve Corrosion Resistance in Boiling Nitric Acid Medium, *Surf. Coat. Technol.*, 2013, **235**, p 45–53
9. M. Jamesh, T.S.N. Sankara Narayanan, and P.K. Chu, Thermal Oxidation of Titanium: Evaluation of Corrosion Resistance as a Function of Cooling Rate, *Mater. Chem. Phys.*, 2013, **138**(2–3), p 565–572
10. P.A. Dearnley, K.L. Dahm, and H. Çimenoğlu, The Corrosion-Wear Behaviour of Thermally Oxidised CP-Ti and Ti-6Al-4V, *Wear*, 2004, **256**(5), p 469–479
11. E. Arslan, Y. Totik, E. Demirci, and A. Alsaran, Influence of Surface Roughness on Corrosion and Tribological Behavior of CP-Ti After Thermal Oxidation Treatment, *J. Mater. Eng. Perform.*, 2010, **19**(3), p 428–433
12. H. Dong, A. Bloyce, P. Morton, and T. Bell, Surface Engineering of Titanium Alloy with Oxygen, *Titanium 95-Science and Technology*, 1996, p. 1999–2006
13. A. Ashrafizadeh and F. Ashrafizadeh, Structural Features and Corrosion Analysis of Thermally Oxidized Titanium, *J. Alloys Compd.*, 2009, **480**(2), p 849–852
14. A.C. Fernandes, F. Vaz, E. Ariza, L.A. Rocha, A.R.L. Ribeiro, A.C. Vieira et al., Tribocorrosion Behaviour of Plasma Nitrided and Plasma Nitrided + Oxidised Ti6Al4V Alloy, *Surf. Coat. Technol.*, 2006, **200**(22–23), p 6218–6224
15. S. Kumar, T.S.N.S. Narayanan, S. Ganesh Sundara Raman, and S.K. Seshadri, Surface Modification of CP-Ti to Improve the Fretting-Corrosion Resistance: Thermal Oxidation Vs. Anodizing, *Mater. Sci. Eng. C. Mater. Biol. Appl.*, 2010, **30**(6), p 921–927

16. D. Siva Rama Krishna and Y. Sun, Effect of Thermal Oxidation Conditions on Tribological Behaviour of Titanium Films on 316L Stainless Steel, *Surf. Coat. Technol.*, 2005, **198**(1–3), p 447–453
17. M. Jamesh, S. Kumar, and T.S.N. Sankara Narayanan, Effect of Thermal Oxidation on Corrosion Resistance of Commercially Pure Titanium in Acid Medium, *J. Mater. Eng. Perform.*, 2012, **21**(6), p 900–906
18. T. Kosec, P. Močnik, and A. Legat, The Tribocorrosion Behaviour of NiTi Alloy, *Appl. Surf. Sci.*, 2014, **288**, p 727–735
19. B. Li, Y. Li, J. Li, X. Fu, C. Li, H. Wang et al., Improvement of Biological Properties of Titanium by Anodic Oxidation and Ultraviolet Irradiation, *Appl. Surf. Sci.*, 2014, **307**, p 202–208
20. Ç. Albayrak, İ. Hacısalihoğlu, S. Yenal Vangölü, and A. Alsaran, Tribocorrosion Behavior of Duplex Treated Pure Titanium in Simulated Body Fluid, *Wear*, 2013, **302**(1–2), p 1642–1648
21. S. Kumar, T.S.N. SankaraNarayanan, S. GaneshSundaraRaman, and S.K. Seshadri, Fretting Corrosion Behaviour of Thermally Oxidized CP-Ti in Ringer's Solution, *Corros. Sci*, 2010, **52**(3), p 711–721
22. M.J. Runa, M.T. Mathew, and L.A. Rocha, Tribocorrosion Response of the Ti6Al4V Alloys Commonly Used in Femoral Stems, *Tribol. Int.*, 2013, **68**, p 85–93
23. A.C. Vieira, A.R. Ribeiro, L.A. Rocha, and J.P. Celis, Influence of pH and Corrosion Inhibitors on the Tribocorrosion of Titanium in Artificial Saliva, *Wear*, 2006, **261**(9), p 994–1001
24. H. Guleryuz and H. Cimenoglu, Effect of Thermal Oxidation on Corrosion and Corrosion-Wear Behaviour of a Ti-6Al-4V Alloy, *Biomaterials*, 2004, **25**(16), p 3325–3333
25. S. Kumar, T.S.N.S. Narayanan, S.G.S. Raman, and S.K. Seshadri, Thermal Oxidation of CP-Ti: Evaluation of Characteristics and Corrosion Resistance as a Function of Treatment Time, *Mater. Sci. Eng. C. Mater. Biol. Appl.*, 2009, **29**(6), p 1942–1949
26. Y. Zhang, D.D. Macdonald, M. Urquidi-Macdonald, G.R. Engelhardt, and R.B. Dooley, Passivity Breakdown on AISI, Type 403 Stainless Steel in Chloride-Containing Borate Buffer Solution, *Corros. Sci.*, 2006, **48**(11), p 3812–3823
27. K.S. Raja and D.A. Jones, Effects of Dissolved Oxygen on Passive Behavior of Stainless Alloys, *Corros. Sci.*, 2006, **48**(7), p 1623–1638
28. Y. Sun and E. Haruman, Effect of Electrochemical Potential on Tribocorrosion Behavior of Low Temperature Plasma Carburized 316L Stainless Steel in 1M H_2SO_4 Solution, *Surf. Coat. Technol.*, 2011, **205**(17–18), p 4280–4290
29. Y.X. Qiao, Y.G. Zheng, W. Ke, and P.C. Okafor, Electrochemical Behaviour of High Nitrogen Stainless Steel in Acidic Solutions, *Corros. Sci.*, 2009, **51**(5), p 979–986
30. Y. Sun, Depth-Profiling Electrochemical Measurements of Low Temperature Plasma Carburised 316L Stainless Steel in 1M H_2SO_4 Solution, *Surf. Coat. Technol.*, 2010, **204**(16–17), p 2789–2796
31. D. Landolt, S. Mischler, and M. Stemp, Electrochemical Methods in Tribocorrosion: A Critical Appraisal, *Electrochim. Acta*, 2001, **46**(24–25), p 3913–3929
32. N.E. Paton and J.C. Williams, *Hydrogen in Metals*, ASM, Metals Park, 1974
33. W. Tsai, C. Ju, Y. Wen, and J. Lee, Hydride Formation During the Cathodic Polarization of Titanium in Artificial Sea Water, *Surf. Coat. Technol.*, 1987, **31**(4), p 401–408
34. P. Millenbach and M. Givon, The Electrochemical Formation of Titanium Hydride, *J. Less Common Met.*, 1982, **87**(2), p 179–184
35. D.S. Shih, I.M. Robertson, and H.K. Birnbaum, Hydrogen Embrittlement of α Titanium: In Situ Tem studies, *Acta Metall.*, 1988, **36**(1), p 111–124
36. S.C. Lee, W.Y. Ho, and T.M. Chen, Prevention of Hydrogen Degradation in Titanium by Deposition of TiN Thin Film, *J. Mater. Eng. Perform.*, 1994, **3**(6), p 740–743
37. X. Jiang, S. Li, C. Duan, and M. Li, A Study of the Corrosive Wear of Ti-6Al-4V in Acidic Medium, *Wear*, 1989, **129**(2), p 293–301
38. Y. Sun and E. Haruman, Tribocorrosion Behaviour of Low Temperature Plasma Carburised 316L Stainless Steel in 0.5 M NaCl Solution, *Corros. Sci.*, 2011, **53**(12), p 4131–4140
39. Y. Sun and V. Rana, Tribocorrosion Behaviour of AISI, 304 Stainless Steel in 0.5M NaCl Solution, *Mater. Chem. Phys.*, 2011, **129**(1–2), p 138–147
40. Z. Jiang, X. Dai, and H. Middleton, Investigation on Passivity of Titanium Under Steady-State Conditions in Acidic Solutions, *Mater. Chem. Phys.*, 2011, **126**(3), p 859–865
41. A. IgualMuñoz and L. CasabánJulián, Influence of Electrochemical Potential on the Tribocorrosion Behaviour of High Carbon CoCrMo Biomedical Alloy in Simulated Body Fluids by Electrochemical Impedance Spectroscopy, *Electrochim. Acta*, 2010, **55**(19), p 5428–5439
42. G. Nakayama, Y. Sakakibara, Y. Taniyama, H. Cho, T. Jintoku, S. Kawakami et al., The Long-Term Behaviors of Passivation and Hydride Layer of Commercial Grade Pure Titanium in TRU Waste Disposal Environments, *J. Nucl. Mater*, 2008, **379**(1–3), p 174–180
43. C.L. Briant, Z.F. Wang, and N. Chollocoop, Hydrogen Embrittlement of Commercial Purity Titanium, *Corros. Sci.*, 2002, **44**(8), p 1875–1888
44. M.J. Frank, M.S. Walter, M.M. Bucko, E. Pamula, S.P. Lyngstadaas, and H.J. Haugen, Polarization of Modified Titanium and Titanium–Zirconium Creates Nano-structures While Hydride Formation is Modulated, *Appl. Surf. Sci.*, 2013, **282**, p 7–16